Ocean Modelling 30 (2009) 256–269

Contents lists available at ScienceDirect

Ocean Modelling

journal homepage: www.elsevier.com/locate/ocemod

High-resolution regional ocean dynamics simulation in the southwestern tropical Atlantic

Marcus Silva [a], Moacyr Araujo [a,*], Jacques Servain [b], Pierrick Penven [c], Carlos A.D. Lentini [d]

[a] Laboratório de Oceanografia Física Estuarina e Costeira, Departamento de Oceanografia da Universidade Federal de Pernambuco (LOFEC/DOCEAN/UFPE), Av. Arquitetura s/n, Cidade Universitária, 50740-550 Recife, PE, Brazil
[b] Institut de Recherche pour le Développement (IRD), UMR-182 Paris, France
[c] Institut de Recherche pour le Développement (IRD), UMR-097 Brest, France
[d] Departamento de Física da Terra e do Meio Ambiente da Universidade Federal da Bahia (UFBA), Campus Ondina, 40170-280 Salvador, BA, Brazil

ARTICLE INFO

Article history:
Received 20 July 2007
Received in revised form 20 May 2009
Accepted 7 July 2009
Available online 15 July 2009

Keywords:
Southwestern tropical Atlantic
Upper ocean
PIRATA-SWE moorings
ROMS
South equatorial current

ABSTRACT

The southwestern tropical Atlantic (05°S–25°S/20°W–47°W), where part of the South Equatorial Current (SEC) enters at its eastern border, is of particular interest as it is fed by many western boundary currents along the eastern Brazilian continental shelf. However, the long-term variability of the dynamics in this region, which are also important as they contribute to the climate over northeastern Brazil, is largely unknown. We use the Regional Ocean Model System (ROMS) here for the first time in this area to simulate the ocean circulation with an isotropic horizontal grid resolution of 1/12° and 40 terrain-following layers. As a primary evaluation of the ROMS configuration, we explore surface and vertical thermal structures, the surface mixed layer, and mass transports within the upper levels. Interannual variability results are compared with the first two-year series of observed thermal profiles derived from the three PIRATA-SWE moorings. The simulated thermal structure in the upper ocean layers agrees well with *in-situ* data. ROMS simulations point out a broad and relatively weak SEC flow composed of a sequence of more or less defined near-surface cores. The westward SEC transport for the upper 400 m along the PIRATA-SWE section, calculated from the ROMS simulation for 2005–2007, shows an average volume transport of 14.9 Sv, with a maximum observed in JFM (15.7 Sv), and a minimum during MJJ (13.8 Sv). ROMS results indicate that the 2005–2007 seasonal near-surface westward SEC transport is modulated by the zonal wind variability. Three zonal sections extending from the American continent to the PIRATA buoy sites confirm that stronger northward NBUC transport and decreasing BC transport were achieved during May 2006 and May 2007, *i.e.* at the time the sSEC bifurcation reaches its southernmost position. On the other hand, the maximum southward BC flow was verified during January 2006, January 2007 and March 2007, with a minimum northward NBUC flow in December 2005 and October/December 2006, corresponding to the period when the sSEC bifurcation reaches its lowest latitude (OND). Sea Surface Height (SSH) and the surface Eddy Kinetic Energy (EKE) derived from simulations and AVISO Rio05 product point out the highest surface meso-scale activity (EKE $\geqslant$ 50 $cm^2\,s^{-2}$) along the cSEC and NBUC/BC patches. Preliminary results provide additional ingredients in the complexity of the SEC divergence region and encourage us to conduct a more detailed exploration of the dynamics of this region using the ROMS. This also shows the need to continue, extend, and vertically upgrade the observational PIRATA-SWE array system, especially with more levels of salinity measurements and the installation of current measurements.

1. Introduction

Surface cold water formation in the North Atlantic and its subsequent plunging to feed the Northern Atlantic Deep Water (NADW), which runs out towards the South Atlantic, are relatively well known (Arhan et al., 1998; Stramma et al., 2005). Paradoxically, the warm counterpart, *i.e.* the subduction formation in the southern hemisphere of shallow warm water and its northward transfer across the equator, is less well understood. The South Atlantic Ocean is of prime importance in global climate change because there are a number of key zones where ocean signals on various timescales (from intraseasonal to decadal) must pass. In the southern subtropical Atlantic basin, which is subjected to both cyclonic and anticyclonic gyres strongly controlled by the surface wind (Stramma and Schott, 1999; Lumpkin and Garzoli, 2005), one can distinguish the following key zones, from South Africa to South America successively:

* Corresponding author. Tel./fax: +55 81 21268225.
E-mail address: moa@ufpe.br (M. Araujo).

1463-5003/$ - see front matter © 2009 Elsevier Ltd. All rights reserved.
doi:10.1016/j.ocemod.2009.07.002

(i) The Agulhas Current off South Africa, coming up from the Indian Ocean and propagating northwards while skirting the African coast;
(ii) the Benguela Current system, including the continuation towards the north of the previous current, and the regional cyclonic circulation within the Angola Dome region;
(iii) the subtropical Atlantic eastward circulation (15°S–20°S, 40°W–20°W), corresponding to an important area of warm and salty water formation by subduction that feeds the South Equatorial Current (SEC), itself formed by at least four easterly branches (the northern branch, nSEC; the equatorial branch, eSEC; the central branch, cSEC; and the southern branch, sSEC) separated by narrow regions of less obvious counter-currents (Stramma, 1991; Stramma and Schott, 1999); and
(iv) more westwards, the zone of divergence of the southern branch (sSEC) of the SEC as it approaches the Brazilian edge.

This latter region is partially responsible for feeding numerous current systems that border the Brazilian coast, towards either the north or the south. Towards the north, the cSEC and sSEC terminations form the North Brazil Undercurrent–North Brazil Current (NBUC–NBC) system, which is one of the most powerful western boundary currents in the world. This system participates in feeding a few other currents (Schott et al., 1995; Bourlès et al., 1999a,b; Stramma et al., 2005); among them, the northward Guyana Current, as well as the eastward North Equatorial Countercurrent and its associated complex retroflection system (Goes et al., 2005), and finally the eastward Equatorial Undercurrent (EUC). Stramma (1991) and Stramma and England (1999) showed that the NBC accounts for approximately one-third of the net warm-water transported across the equatorial tropical gyre boundary into the North Atlantic, compensating for the southward export of NADW. After the bifurcation close to the Brazilian shelf, the sSEC also feeds the Brazil Current (BC), propagating southward along the coast of Brazil (Stramma, 1991; Peterson and Stramma, 1991; Stramma et al., 1995) and meeting the Malvinas Current at about 35°S (Gordon and Greengrove, 1986; Olson et al., 1988; Garzoli and Garrafo, 1989), which itself is fed in part by cold water coming from the Pacific Ocean via Drake's passage.

The latitude where the sSEC bifurcation occurs is not well known, although it has been demonstrated from observation and model results (Silveira et al., 1994; Stramma et al., 1995; Rodrigues et al., 2007) that the North Brazil Undercurrent (NBUC) originates south of 10°S.

The SEC as a whole, where the present study is focused (Fig. 1), has a potential climatic influence in several remote regions: (i) mainly in the northward direction through its participation in the NBC–NBUC system and its derived complex system (Talley, 2003; Ganachaud, 2003; Lumpkin and Speer, 2003) and (ii) also in the southward direction through its effect on the Brazil–Malvinas Current confluence and the return of the South Atlantic gyre (Stramma and Peterson, 1990; Peterson and Stramma, 1991). Furthermore, as it is in the region of the southeast trade winds and the South Atlantic Convergence Zone (SACZ), interactions between sea surface temperature (SST) and the easterly atmospheric circulation may play a significant role in local climate fluctuations of northeastern Brazil, a region affected by intermittent severe droughts and floods (Moura and Shukla, 1981; Rao et al., 1993).

We are mainly interested here in analyzing the accuracy of a versatile new generation state-of-the-art Regional Ocean Modeling System (ROMS) as it reproduces some aspects of intraseasonal to interannual ocean dynamics in the region of the southernmost extent of the westward SEC. Thanks to its refined spatial resolution (1/12° = 9.25 km in latitude and longitude; 40 vertical levels, of which 20 are from surface to 500 m depth) one should expect that

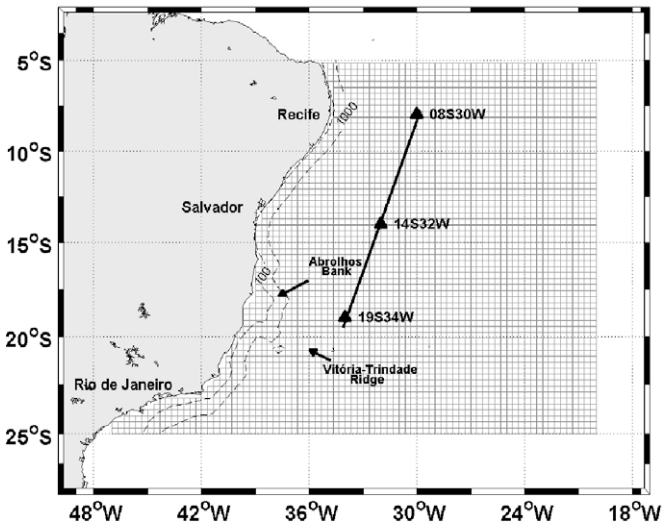

Fig. 1. Model domain (grid) and PIRATA-SWE buoy locations (triangles) along the western boundary. The 100 and 1000 m isobaths are represented by the two dashed lines. Section across PIRATA-SWE buoys (solid black line).

ROMS resolves the thermohaline properties and meso-scale dynamics in the study region that cannot be resolved when using OGCMs with lower resolutions.

We first compare the model results with both instantaneous and rare available long-term observations. Continuous subsurface observations in this study region were non-existent until the recently deployed ATLAS buoys in August 2005 as part of the South West Extension of the Pilot Moored Research Array in the Tropical Atlantic (PIRATA-SWE) (Servain et al., 1998; Bourlès et al., 2008; Nobre et al., 2005), which runs along the edge of Brazil's coastline south of the equator (Fig. 1). Therefore, this work intends also to refine the arguments for a continuation, and even extension, of the oceanic observing system in this region.

The main characteristics of ROMS and conditions of the interannual simulation are presented in the next section, while Section 3 gives some details of the PIRATA-SWE observation dataset. The ROMS evaluation is performed in Section 4 by comparing outputs of the model to high-frequency observed SST fields estimated by satellite, thermal structures and mixed layer depths provided by the PIRATA-SWE dataset. As a first dynamical application of ROMS, Section 5 shows examples of the simulated variation of mass transports across three zonal transects, and the section along the PIRATA-SWE sites. The last section presents a conclusion and perspectives.

2. The model simulation

ROMS is an ocean model (Shchepetkin and McWilliams, 2005) previously adapted to different regions of the world ocean (Haidvogel et al., 2000; Malanotte-Rizzoli et al., 2000; She and Klinck, 2000; Penven et al., 2000, 2001a,b; McCready and Geyer, 2001; Lutjeharms et al., 2003). The model solves the free surface primitive equations in an Earth-centered rotating environment based on the classical Boussinesq approximation and hydrostatic vertical momentum balance. ROMS is discretized in terrain-following vertical coordinates. The model grid, forcing, initial and boundary conditions were built using the ROMSTOOLS package developed by the Institut de Recherche pour le Développement (IRD) (Penven et al., 2008). Upstream advection is treated with a third-order scheme that enhances the solution by generating steep gradients as a function of a given grid size (Shchepetkin and McWilliams, 1998).

Unresolved vertical subgrid-scale processes are parameterized by an adaptation of the non-local K-profile planetary boundary layer scheme (Large et al., 1994). A complete description of the model can be found in Haidvogel et al. (2000) and Shchepetkin and McWilliams (2005).

The case study presented here involves the open ocean area near the NE Brazilian coast. The integration domain is from 5°S to 25°S and 20°W to 47°W (Fig. 1). We use an isotropic 1/12° horizontal grid with 323×249 horizontal mesh cells and a vertical discretization of 40 levels. Bottom topography was derived from a 2′ resolution database ETOPO2 (Smith and Sandwell, 1997), and a slope parameter $r = \nabla h/h < 0.20$ was used to prevent errors in the computation of the pressure gradient (Haidvogel et al., 2000). At the three open boundaries (north, east and south), an active, implicit, upstream-biased radiation condition connects the model solution to the surrounding ocean (Marchesiello et al., 2001). Horizontal Laplacian diffusivity inside the integration domain is zero, and a 12-point smoothing scheme is imposed (up to $10^4\ m^2\ s^{-1}$) in the sponge layers near the open ocean boundaries. The model equations are subjected to no-slip boundary conditions along the coastline. The oceanic circulation was forced at the sea surface by monthly-averaged heat and fresh water fluxes derived from COADS (da Silva et al., 1994) and daily-mean (2005–2007) wind stress by QuickSCAT (Liu, 2002). A basin-scale daily-mean (2005–2007) hydrography and currents derived from OGCM–ECCO (http://ecco.jpl.nasa.gov/) are used to infer thermohaline properties and water volume exchanges at the open horizontal boundaries. The model simulation was performed in two steps. First, the rested ocean was gradually forced by applying ramp functions to the boundary conditions for the period January–December 2001. After this, the full sets of forcing conditions for 2001–2007 were considered for the interannual simulation.

3. The PIRATA-SWE observation dataset

The PIRATA Southwest Extension (PIRATA-SWE) was proposed as an extension of the original PIRATA array (Servain et al., 1998) in order to understand the seasonal and interannual variability over the southwestern tropical Atlantic. Its primary objective is to help the forecast of the Brazilian climate, especially over the northeastern part of Brazil. Therefore, and in accordance with several scientific arguments proposed by Nobre et al. (2005) and Bourlès et al. (2008), three sites were chosen for the ATLAS mooring buoys along the NE Brazilian coast: (i) at 8°S–30°W in connection with the 0°N–10°W mooring site of PIRATA's original array; (ii) at 14°S–32°W in connection with the SEC flow variability; and (iii) at 19°S–34°W in connection with the South Atlantic Convergence Zone (Fig. 1). We note that the PIRATA-SWE array only addresses the changes in the thermohaline structure within the SEC's flow into the bifurcation region. Understanding changes in the partition between the North Brazil Current (NBC) and the Brazil Current (BC) at the SEC bifurcation region is not within the scope of PIRATA-SWE's objectives.

The three ATLAS buoys in PIRATA-SWE were launched for the first time in late August 2005, following the same mooring design used in the original array of PIRATA's buoys. Daily transmissions of ocean temperature at 11 levels (1, 20, 40, 60, 80, 100, 120, 140, 180, 300, and 500 m), salinity at 4 levels (1, 20, 40, and 120 m), and meteorological variables at the sea surface are collected and transmitted via the Argos satellite system, and are immediately made available on the web after their validation (http://www.pmel.noaa.gov/pirata/).

The PIRATA-SWE buoys were selected in an attempt to compare and validate the model results at the subsurface. Therefore, only the first two years of the PIRATA-SWE dataset for 0–500 m of temperature vertical profiles were used. While the daily data return of the ATLAS mooring located at 14°S–32°W is nearly 100%, the two other buoy sites experienced a few technical failures. For instance, automatic measurements at the 8°S–30°W location were interrupted on June 24th 2006 due to an anchoring problem. This dataset was again made available only after November 2006. The southernmost site, located at 19°S–34°W, also experienced a technical failure in some of its subsurface sensors in November 2006, but as shall be explained in Section 4.2, essential information regarding its temperature vertical distribution could be retrieved thanks to an interpolation scheme.

4. Thermal structure in the southwestern tropical Atlantic

4.1. Instantaneous SST evaluation

As a preliminary test to validate the numerical results, we evaluated the model accuracy by comparing daily SST surface maps derived from the ROMS model to daily infrared SSTs derived from the GODAE High Resolution SST Pilot Project (GHRSST-PP, 2007). This comparison was done for two different scenarios: September 15th 2005, which corresponds to the austral winter, and March 15th 2006, which corresponds to the austral summer (Fig. 2). The satellite-derived SST maps have a horizontal resolution of 9.25 km. A full description of the GHRSST-PP can be found on the GHRSST-PP website at http://www.ghrsst-pp.org.

In the region of interest, the model and satellite daily SST patterns are consistent, showing a distinct meridional seasonal change along the South Atlantic western boundary. The so-called Southwestern Atlantic Warm Pool (SAWP) (Huang et al., 1995; Nobre et al., 2005), which is marked by high SST values (>27 °C), extends off the South American coastline from the equator to about 12°S on September 15th, 2005, which includes the northern part of the PIRATA-SWE (Fig. 2a and b). Six months later, on March 15th, 2006, these high SST values invade the whole area of study, and warmer waters are observed at the three PIRATA buoy sites (Fig. 2c and d). Besides its meridional seasonal migration, the SAWP pattern also records seasonal zonal changes with a more eastward extension during the summer, especially in the northern part. The seasonal spreading out of cold waters (<22 °C) in the open ocean at the southern limit of the study domain follows the same meridional progression as that observed for the SAWP. These cold waters are advected off the southern limit of the study area in March.

Besides the fact that the model accurately reproduces the satellite-derived SST overall, it also resolves the meso-scale dynamical processes quite well, including frontal structures, meanders and local upwelling regions. For instance, the cold water filaments observed in the model outputs for March 15th, 2006 in the vicinity of the Abrolhos Bank (Lat. 17–18°S—Long. 38.5°–39.5°W) and the Vitória-Trindade Ridge (Lat. 20°S—Long. 34–38°W) are good indicators of observed and modeled upwelled waters and meso-scale cyclonic structures previously documented in this area (Schmid et al., 1995; Campos, 2006). Indeed, the modeled SST is especially efficient compared to the satellite-derived SST estimates along the coastline where the infrared retrievals may be cloud-contaminated. Although the horizontal resolution of the model and the GHRSST-PP SST product are almost the same (~10 km), the fine meso-scale surface structures evident in the model results seem to be smoothed in the infrared SST maps. This is probably due to the fact that several individual images and infrared products are combined and used to estimate the SST. For example, it does not seem random that higher differences between satellite and modeled SST are present in late austral summer close to the coastal region between 16°S and 22°S (Fig. 2c and d); this is a well-known

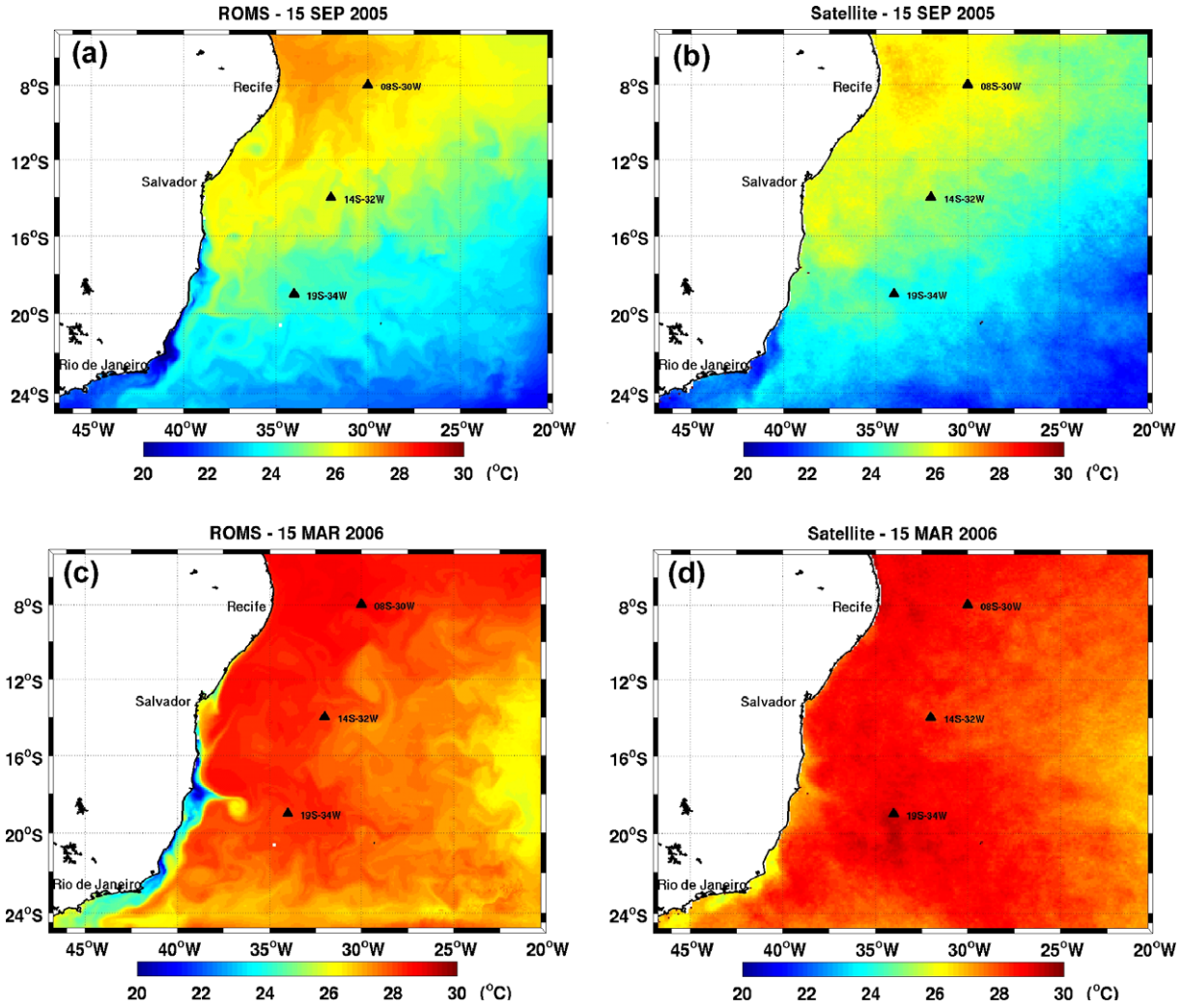

Fig. 2. Comparison between ROMS-derived SST (a and c) and GHRSST-PP-derived SST (b and d) for September 15th 2005 and March 15th 2006.

cloudy area under the influence of the atmospheric South Atlantic Convergence Zone—SACZ (Chaves and Nobre, 2004; De Almeida et al., 2007).

4.2. Seasonal (2005–2007) evaluation of the subsurface temperature and mixed layer depth

In this second set of model evaluations, samples of local time series of the vertical distribution of temperature given by ROMS are directly compared to the first available two-year period dataset provided by PIRATA-SWE. Fig. 3a–c primarily shows the simulated and observed variations of the 0–500 m temperature profile (September 2005–June 2007) for the three PIRATA-SWE locations (08°S–30°W, 14°S–32°W and 19°S–34°W). The modeled temperature is represented by black contours (for a two-day period), while the PIRATA temperature appears as white contours (also for a two-day period), and shaded colors (daily). Vertical interpolations were processed on the PIRATA data when only one out of three consecutive temperature sensors along the moored line was dysfunctional. That was the case for the first 50 m level at the 08°S–30°W mooring site from 10 November 2006 to the end of June 2007, as well as for the levels below 180 m at the 19°S–34°W mooring from 3 November 2006 to the end of June 2007. At the 08°S–30°W, missing values are represented by unshaded areas, and at 19°S–34°W, missing values were interpolated between 140 m and 300 m levels.

ROMS reproduces well the tightening of the thermocline for most of the northernmost PIRATA-SWE site (08°S–30°W, Fig. 3a), and the relaxation of the vertical gradient for the two southernmost sites (Fig. 3b and c). In terms of the seasonal cycle within the mixed layer, the simulated and observed cores of the warmest (>28 °C for the near equatorial site, >26 °C for the two other sites) shallow waters (0–75 m) occur within the same period of the year. There are, however, a few episodic discrepancies between ROMS and the PIRATA-SWE data in the levels including the thermocline and the layer depths from ~75 to ~200 m for the northernmost site, and from ~100 to ~250 m or even more for the two other sites. For most of these differences, the 26- to 16 °C isotherm depths given by the model are shallower than the PIRATA-SWE observations, extending from a few meters (*e.g.*, the northern site) to a few tens of meters (*e.g.*, the 20 °C isotherm depth for a few episodes at the central and southern sites). This indicates a relatively permanent cold bias in the model for these depths, which can vary from 0.8 °C at 08°S–30°W to more than 2 °C at 19°S–34°W at the most. These discrepancies are probably due to the model's difficulty in accurately reproducing the ventilation of subducted lower-thermocline waters coming from the subtropical South Atlantic Ocean. For the lower levels (*e.g.*, ~16- to 12 °C isotherms) the model again becomes generally consistent with the observations.

The PIRATA-SWE data clearly show intraseasonal variations of the thermocline depth within a 3–4 month periodicity, especially

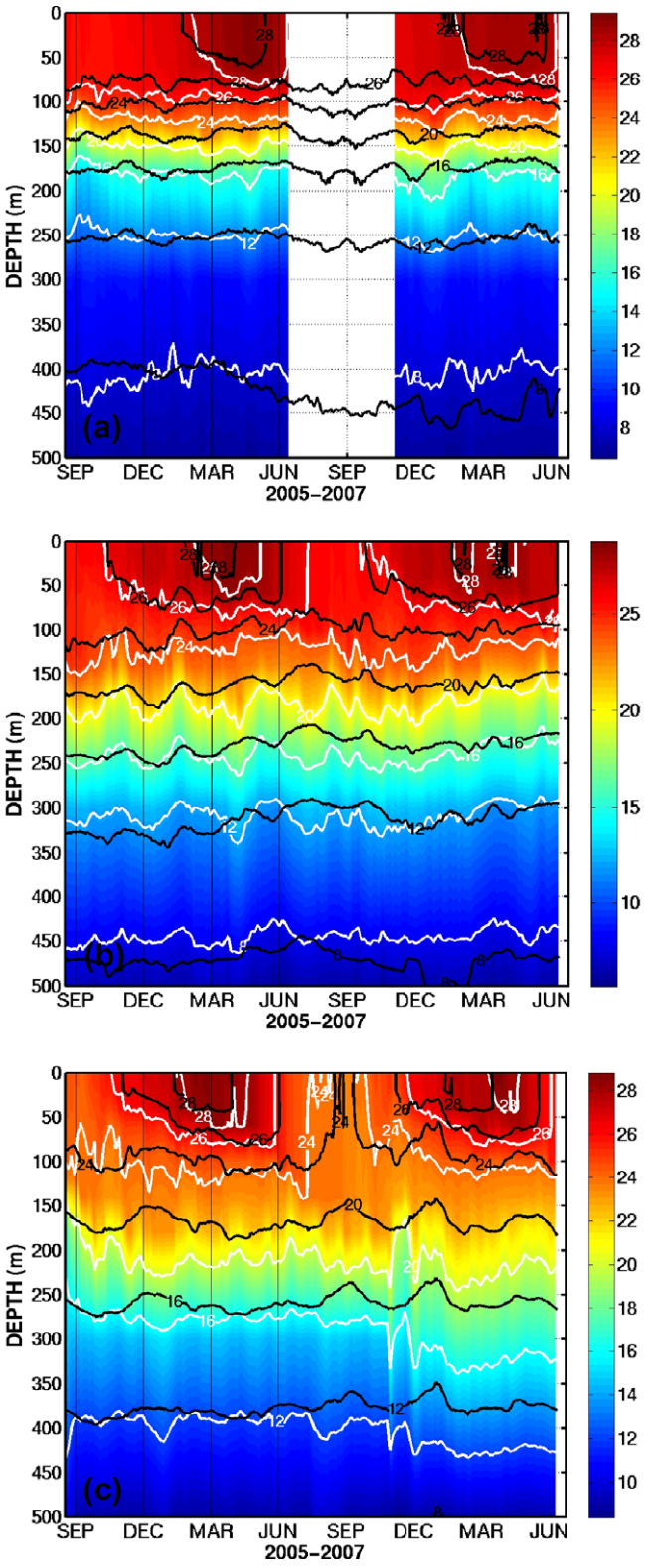

Fig. 3. Comparison between simulated and observed temperature (°C) variations for the upper 500 m from September 2005 to July 2007 for the three PIRATA-SWE locations at (a) 08°S–30°W, (b) 14°S–32°W and (c) 19°S–34°W. Model-derived temperature is represented by black contours and the PIRATA-SWE observed temperature appears as white contours and shaded colors.

for the central and southernmost locations (Fig. 3b and c). This observed variability may be partially explained in terms of an ocean adjustment to disturbances in the buoyancy field due to the propagation of Tropical/Kelvin-Helmholtz instability waves (Proehl, 1996; Polito and Cornillon, 1997; Jochum et al., 2004). These disturbances cause the vertical displacement of the isotherms and propagate equatorward keeping the coastal boundary to the left in the southern hemisphere. Of great interest here is the apparent capacity for ROMS to generate such variability in the temperature profile (see the black lines of Fig. 3b and c around the 20 °C isotherm depth), even if simulated and observed fluctuations are not always in phase.

In order to gain better insight into the preceding discussion, four selected monthly mean temperature profiles (0–500 m) computed from ROMS outputs are compared to the observational data derived from the three PIRATA-SWE moorings for the same months (Fig. 4), *i.e.* September and December 2005 and March and June 2006. For most of the 12 temperature profiles (also marked by vertical black lines in Fig. 3), the model and observations are in good agreement. This is especially the case during the first two months (September and December 2005), where a cold bias, such as those previously discussed, occurs in September 2005 at 14°S–32°W within 100–250 m, and in December 2005 at 19°S–34°W within 50–300 m. Other examples of limited negative biases are observed in March and June 2006 at these same depths.

We conclude this subsection with an evaluation of the temporal evolution of the mixed layer depth (MLD) for both the model runs and the observations. Following Sprintall and Tomczak (1992), we computed the MLD in terms of temperature and density steps (see Appendix A for details). Note that for these calculations, the number of available levels for the modeled temperature and salinity is 20 for the first 300 m, *i.e.* two (five) times the temperature (salinity) number of levels of the PIRATA-SWE data for the same depth. Fig. 5 shows the simulated and observed temporal evolutions of the MLD from September 2005 to July 2007 according to the ROMS outputs (solid lines) and the *in-situ* PIRATA-SWE measurements (dashed lines). The ROMS-derived MLD *vs.* the PIRATA-SWE-derived MLD shows a similar pattern between the model and the observations with a few discrepancies that are more pronounced at the 8°S–30°W mooring site. The calculated cross-correlation coefficients between observed and modeled MLD signals are 0.65 (8°S–30°W), 0.45 (14°S–32°W) and 0.71 (19°S–34°W) (95% confidence level and 321 degrees of freedom). The cross-correlation coefficient is a measure of similarity between the signals. Quite good agreement is evident and the observed and simulated MLD curves have similar shapes, ranging from small values (~30–60 m) during the austral summer, to large values that reach up to 100 m at the end of the austral winter. Note that the PIRATA-SWE-derived MLD was not plotted at 19°S–34°W from 10 May to 11 November 2006 due to missing salinity observations in the upper level. Perhaps the largest difference for the MLD estimation between ROMS and *in-situ* data is noticed here at the 08°S–30°W site (Fig. 5a). Indeed, even if the seasonal evolutions are in phase, the simulated MLD is generally systematically shallower (from 0 to about 30 m) than the observational data. This feature is already visible in Fig. 3, where the ROMS 26 °C isotherm depth at 08°S–30°W is always significantly shallower. The systematic underestimation of the MLD at 08°S–30°W seems to be related to the difficulty on estimating observational MLD. The vertical measurements of salinity on the ATLAS moorings are presently limited to only four levels (1, 20, 40, and 120 m) within the upper layer (see Section 3). Another reason to this discrepancy can be related to the use of climatological heat flux to forcing surface layer. One way to investigate this last hypothesis is through a series of case studies to check the model's sensitivity to different forcings. These additional analyses are outside the scope of this preliminary ROMS evaluation.

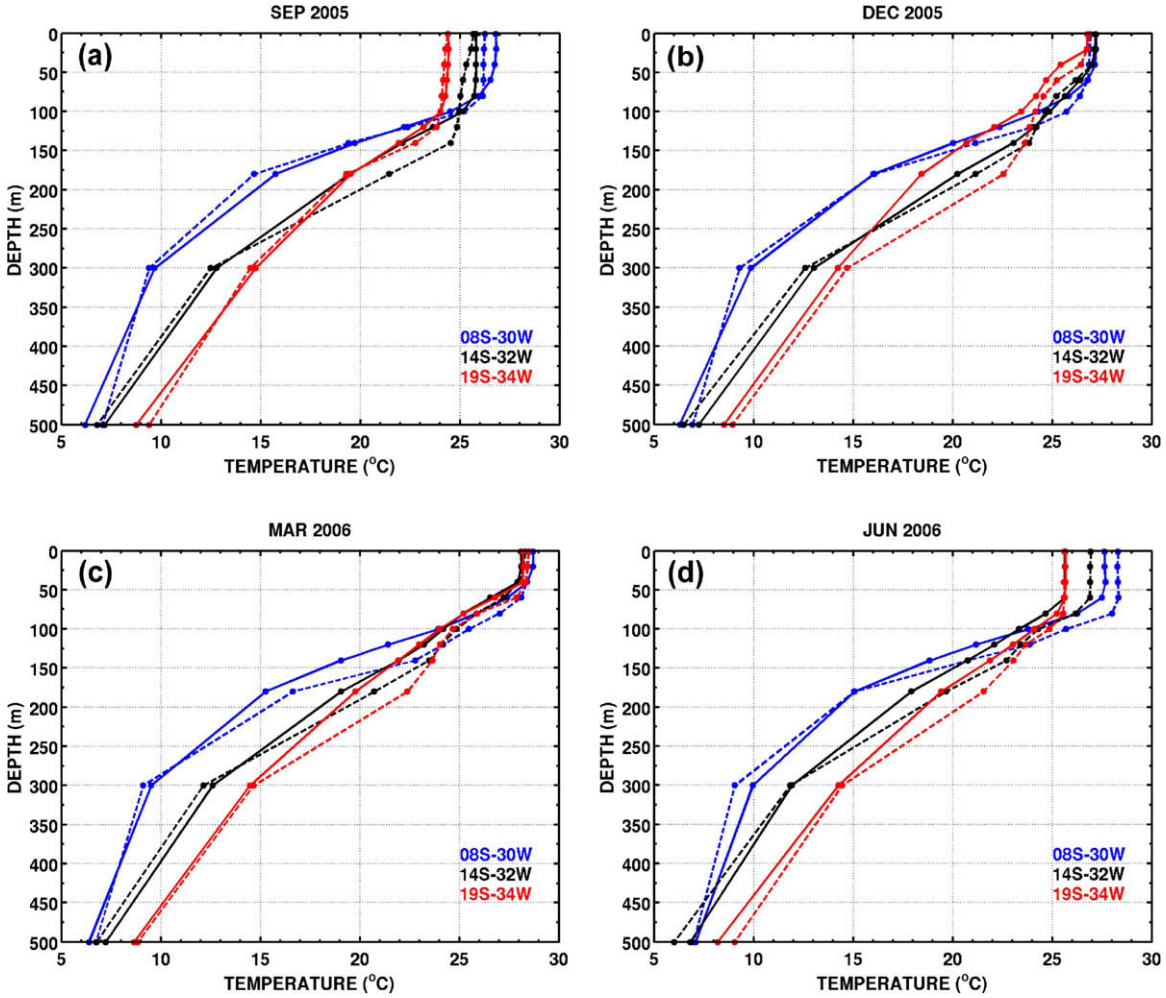

Fig. 4. Comparison of monthly averaged vertical profiles of temperature for the first 500 m between the PIRATA-SWE *in-situ* observations (dashed line) and the ROMS simulation (solid line) for: (a) September 2005, (b) December 2005, (c) March 2006 and (d) June 2006. Colors are associated with each PIRATA-SWE buoy: 08°S–30°W (blue), 14°S–32°W (black) and 19°S–34°W (red). (For interpretation of color mentioned in this figure the reader is referred to the web version of the article.)

5. Transport and pathways in the southwestern tropical Atlantic

5.1. Meso-scale activity in the southwestern tropical Atlantic

The averaged (2005–2007) simulated Sea Surface Height (SSH) and the derived surface Eddy Kinetic Energy (EKE) of the study area are presented in Fig. 6a–d. In these figures, the numerical results are compared to the AVISO Rio05 product for the same periods. Mean SSH was obtained from AVISO Rio05, combining hydrographic data, surface drifters velocities, altimetry and a geoid model (Rio and Hernandez, 2004). Simulated and measured surface Eddy Kinetic Energy (EKE) were calculated from SSH gradients with a similar temporal sampling.

The ROMS-simulated boundary systems (Fig. 6a and b, respectively) bear good resemblance to those of AVISO Rio05 data (Fig. 6c and d). The similarity of the isocontours as well as the eddy-induced structures along the BC is particularly strong. The highest values are greater than 50 $cm^2\ s^{-2}$, found in cSEC and the NBUC/BC areas; this holds for both AVISO Rio05 and ROMS. In general, observations show stronger meso-scale activities in the southwestern tropical Atlantic boundary as compared to the ROMS simulation, but the geographic patterns are similar. It is possible to identify three common characteristic areas of high surface variability that are present in ROMS and AVISO Rio05 EKE charts: the near-shore BC patch south of 16°S, where meso-scale cyclonic structures are documented (Schmid et al., 1995; Campos, 2006), along the Brazilian edge north of Salvador, following the NBUC jet, and the zonal band close to the northernmost boundary of the integration domain (5–6°S), where the central branch of the SEC develops (Lumpkin and Garzoli, 2005). Concerning the coastal region, SSH (and consequently EKE) maps indicate that the NBUC/BC proper is not well represented in AVISO Rio05 dataset. This is probably associated with the partial inability of the altimetry data to accurately capture part of the strong boundary current inertia near the coastline.

5.2. Seasonal (2005–2007) variability of the sSEC/NBUC/BC system

The simulated volume transport in Sv (1 Sv = $10^6\ m^3\ s^{-1}$) of the sSEC/NBUC/BC system between the surface and 600 m is shown in Fig. 7a and b for the averaged period of MJJ and OND (2005–2007), respectively. The first characteristic of ocean circulation expressed in Fig. 7a and b is the inclination of the transport isolines during MJJ compared to the OND period. Indeed, during OND, when less intense SW trade winds are present, the transport lines west of 24°W approach the continent at more or less constant latitudes. In this case, the southern branch of the SEC, which carries 5 Sv, reaches the coast at about 16°S, while the transport isoline of 10 Sv approaches the land near 10°S. Even during MJJ, characterized by more intense action of the SW trades, the transport isolines

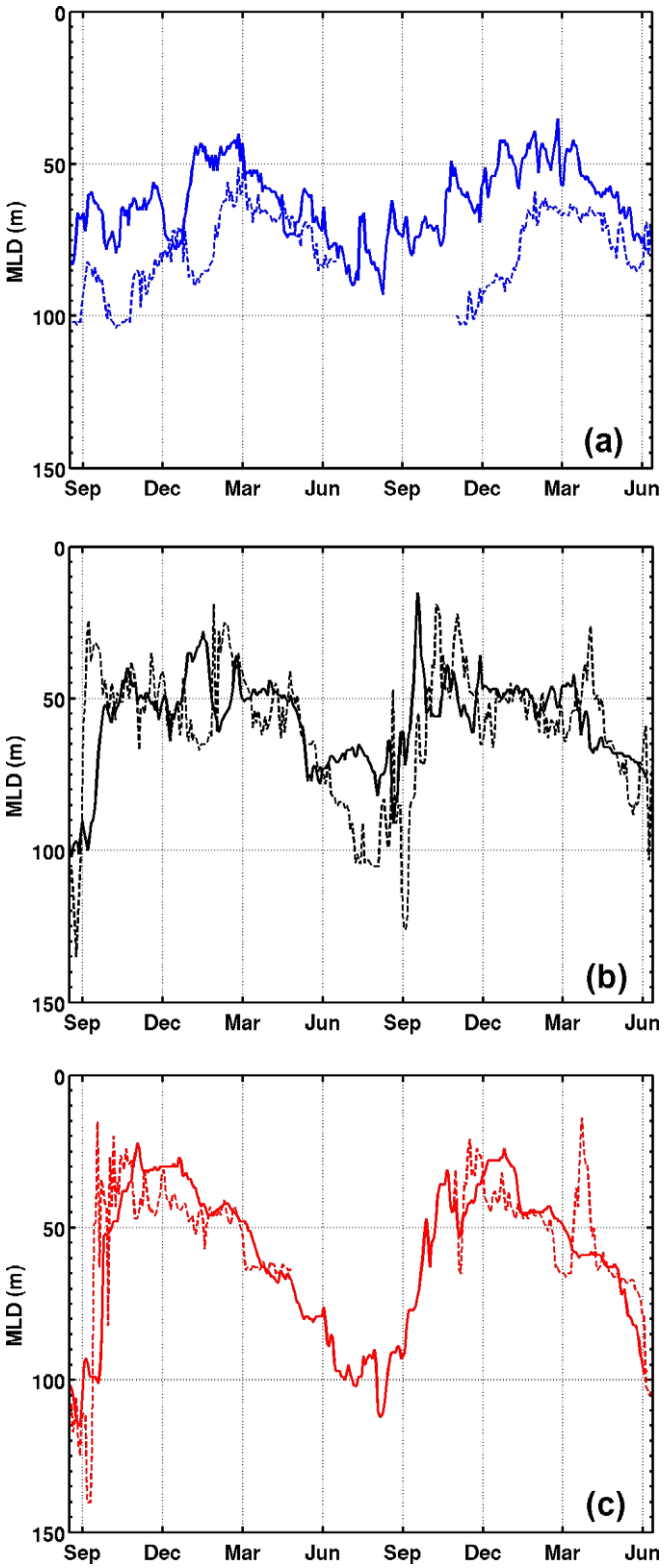

Fig. 5. Comparison of temporal evolution of the seasonal (2005–2007) mixed layer depth (MLD) at: (a) 8°S–30°W, (b) 14°S–32°W and (c) 19°S–34°W, provided by PIRATA-SWE *in-situ* observations (dashed line) with ROMS (solid line) for the period of September 2005 to July 2007.

of 5 and 10 Sv are clearly tilted in relation to the parallels, approaching the edge of the continental shelf around 18°S and 14°S, respectively. Through these figures, we can also see a strengthening of the alongshore NBUC transport during the period in which the isolines reach the coast further south, with simultaneous weakening of the transport of BC to the south (MJJ, Fig. 8a). The inverse situation is observed in Fig. 7b (OND), when the bifurcation of sSEC occurs further north. In this case, the NBUC is weakened and the BC is intensified (see also Fig. 11a and b).

Meridional current and transport estimates averaged for the period of September 2005 to July 2007 are presented here along zonal sections (0–1500 m) at 8°S, 14°S and 19°S, which correspond to the latitudes of the three PIRATA-SWE buoys (Fig. 8a–c). Three σ_t levels are selected according to the local dynamics. The first sigma level ($\sigma_t = 24.5$ kg m^{-3}) separates the upper Tropical Surface Water (TSW) from the upper thermocline waters. The second sigma level ($\sigma_t = 26.8$ kg m^{-3}), which is located at about 150 m, is the lower level of the water supplying the EUC (Schott et al., 1998). The third one ($\sigma_t = 32.15$ kg m^{-3}), which corresponds to ~1000 m, indicates the lower boundary of the upper warmer waters as well as the lower boundary of the Antarctic Intermediate Water (AAIW). Below a depth of 1100 m, we found the North Atlantic Deep Water (NADW) extending to about 4000 m. This is the layer where the Deep Western Boundary Current (DWBC) transports southward cold waters from the northern hemisphere.

The zonal mean sections in Fig. 8a–c show a clear representation of the NBUC skirting the coastline from 100 to 1000 m, with a northward transport increasing from 6.7 Sv at 19°S to 20.3 Sv at 8°S. Along the latitude of 8°S, the core of the NBUC is located about 50 km from the coast, at approximately 50 to 600 m depth (Fig. 8a), and between 250 and 650 m depth at 14°S (Fig. 8b) and at 19°S (Fig. 8c). Still, in the first 1500 m, the presence of a mean southward flow east of the lower NBUC is observed from the model transects at 8°S and 14°S (*i.e.* 150 and 350 km from the coast, respectively), suggesting a continuous offshore recirculation branch at depths between 200 and 1400 m. The southward transports of 2.3 Sv at 8°S and 4.3 Sv at 14°S (Fig. 8a and b) were also found in the LADCP measurements and EOF analysis performed by Schott et al. (2005) and Schuckmann (2006), who found mean representative values of −5.2 ± 4.9 and −4.1 ± 3.7 Sv at 5°S (ship sections) and 11°S (ship sections + mooring array), respectively. There are three possible explanations for the origin of this flow. One could be the deflection of zonal currents. However, no evidence for a southward deflection has been reported in the literature for these currents, because the South Equatorial Undercurrent and the Southern Intermediate Countercurrent transports stay nearly constant between 35°W and 28°W (Schott et al., 2005). A second explanation for this southward flow located east of the NBUC is an inflow from the east as part of the deep cSEC, which gets deflected southward before reaching the Brazilian coast, and thus forms an offshore counterflow (hereinafter referred as CFLOW) to the deep NBUC. Furthermore, the flow could be explained by a retroflection of the deep NBUC just a little bit north of the northeastern tip of Brazil to supply the southward offshore flow across 5°S, identified in the high resolution (1/12°) MICOM model simulation (Schott et al., 2005). In order to investigate these hypotheses, we plotted in Fig. 9 the annual averaged (2005–2007) meridional current (cm s^{-1}) and transport (in Sv) obtained by ROMS for: (a) the along zonal section (0–1500 m) at 7°S, and (b) the depth range of 200–1000 m, where southward CFLOW is stronger (see Fig. 8a and b). Despite the proximity of the northern boundary of the integration domain (and as a consequence, of the influence of the numerically-imposed sponge layer condition between 5 and 6°S), our modeling results plead in favor of the second case mentioned above, *i.e.*, that the offshore counterflow to the deep NBUC is fed by the southernmost limb of the deep cSEC.

Further east of the CFLOW (−2.3 Sv) shown in Fig. 8a, we can distinguish two main current systems, one to the north with a corresponding transport of 2.1 Sv from 200 to 300 km away from the coast, and another to the south (−3.5 Sv) located between 300 and

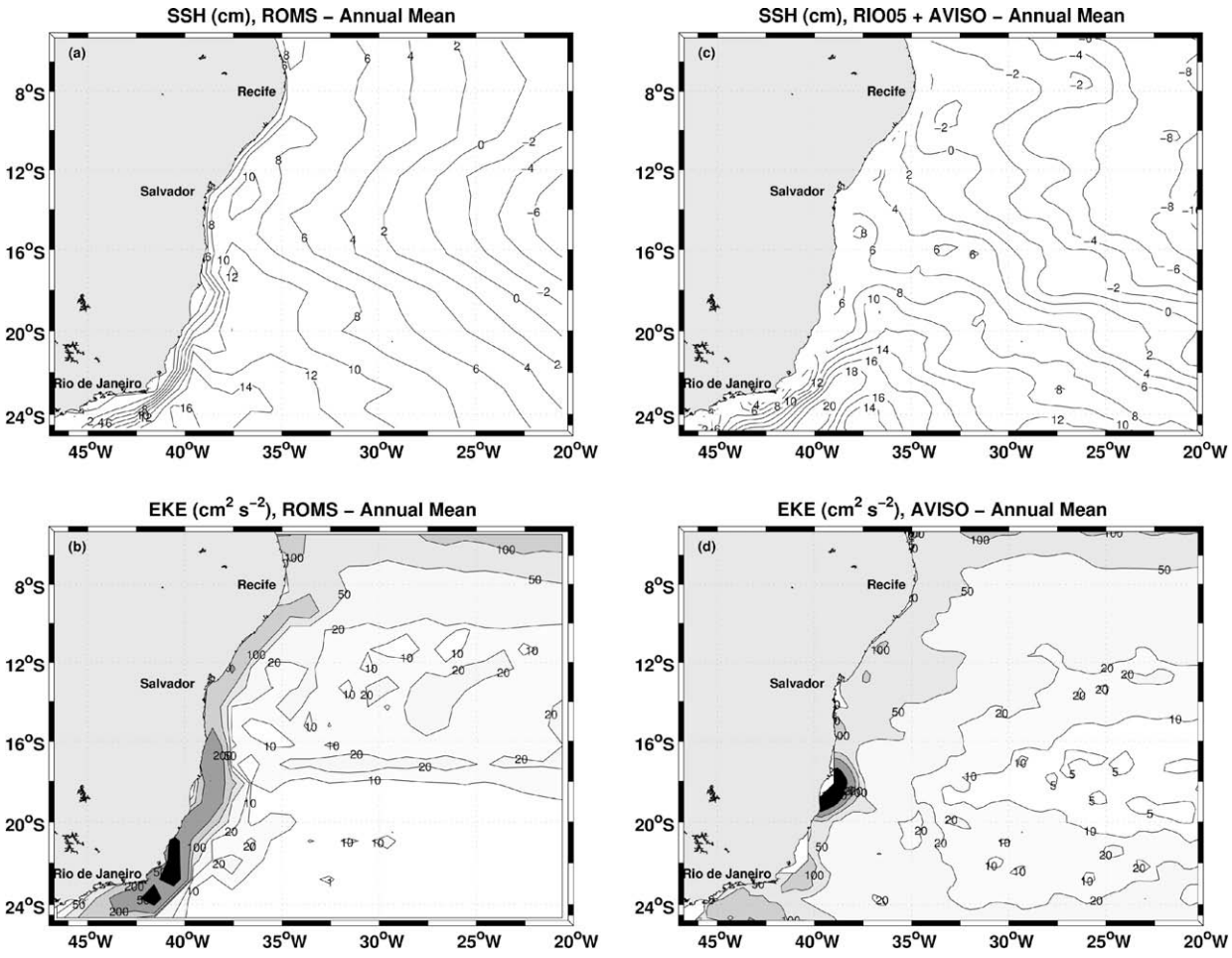

Fig. 6. Averaged (2005–2007) SSH and EKE comparisons between ROMS simulations and AVISO Rio05 data: (a) ROMS – SSH (cm), (b) ROMS – EKE (cm^2 s^{-2}), (c) RIO05 + AVISO – SSH (cm) and (d) AVISO – EKE (cm^2 s^{-2}).

500 km from the shoreline. These meridional offshore cores were also found by Schott et al. (2005) between the 9ºS and 11ºS transects.

The southward-flowing BC, confined to the shallow and nearshore part of the Brazilian continental slope, is especially recognizable at the 19°S section with a mean transport of −2.8 Sv and meridional velocities ranging between 10 to 20 cm s^{-1} (Fig. 8c). Miranda and Castro (1981) identified the BC at 19°S as a surface narrow current (~75 km) limited to the upper 500 m. Evans et al. (1983) indicate that the BC remains confined and organized as a coherent flow above the continental shelf at 20.5°S. The World Ocean Circulation Experiment (WOCE) current-mooring measure-

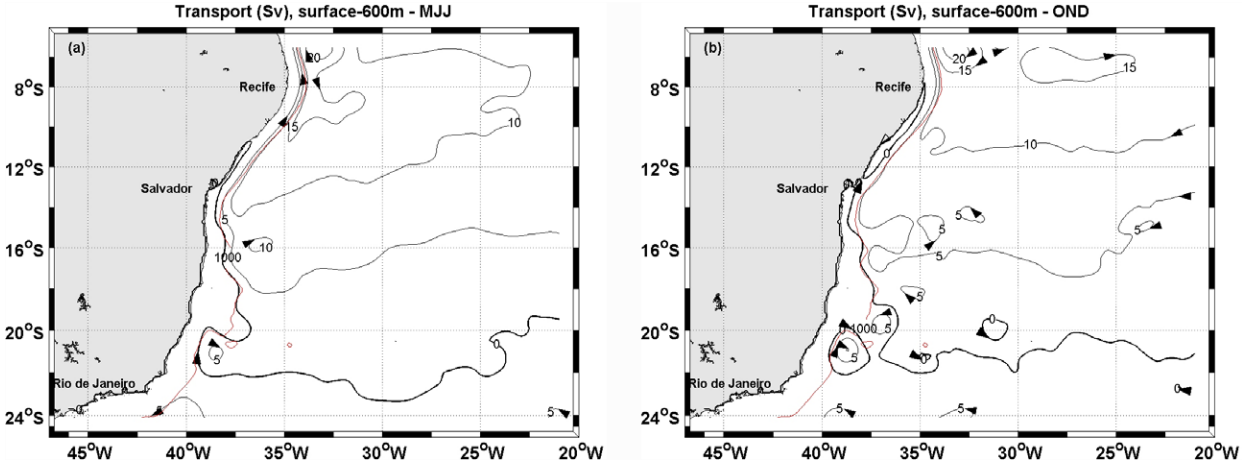

Fig. 7. Transport function (Sv) for the modeled seasonal averaged (three months, 2005–2007) currents integrated from 600 m to the sea surface for (a) MJJ and (b) OND. The 1000 m isobath is represented by a red line. (For interpretation of color mentioned in this figure the reader is referred to the web version of the article.)

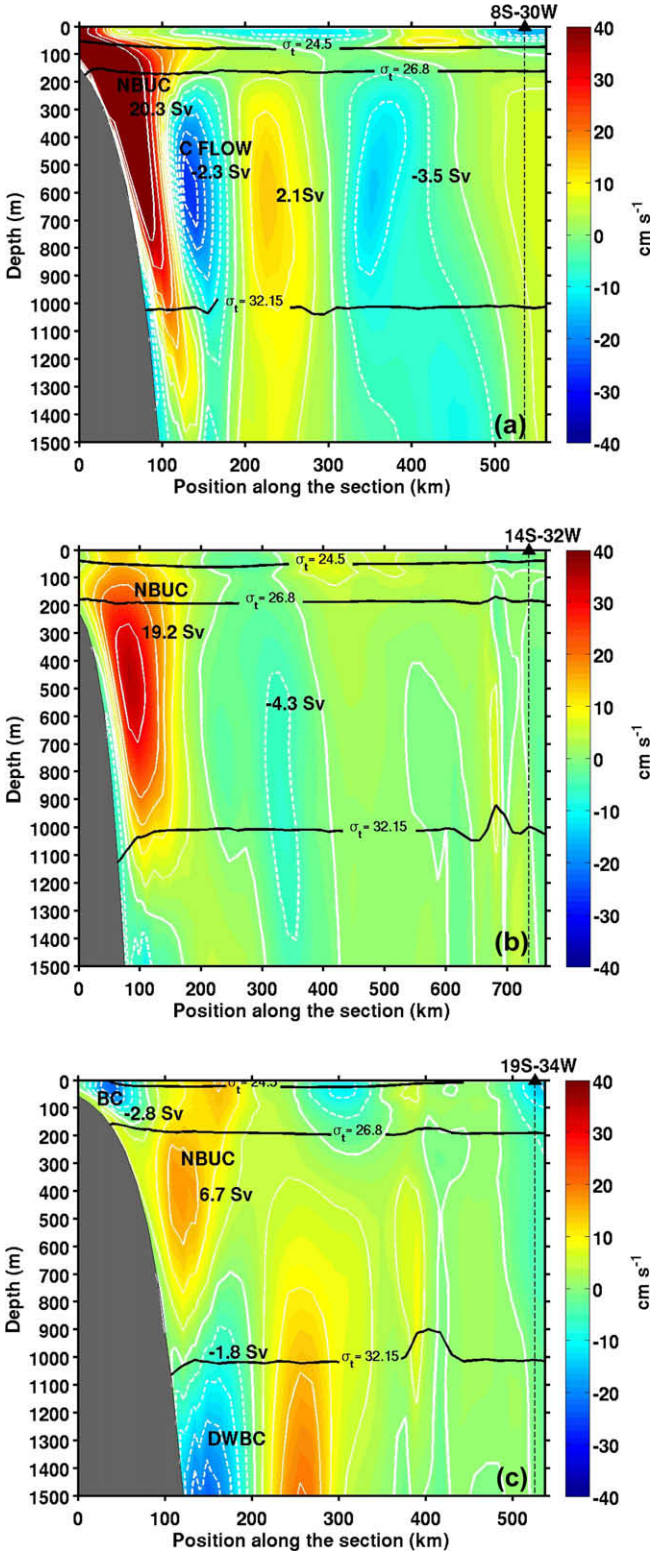

Fig. 8. Model simulation of meridional current and transport values averaged from September 2005 to July 2007 along zonal sections (0–1500 m) at: (a) 8°S, (b) 14°S and (c) 19°S. Positive (negative) values indicated by solid (dashed) lines correspond to northward (southward) currents.

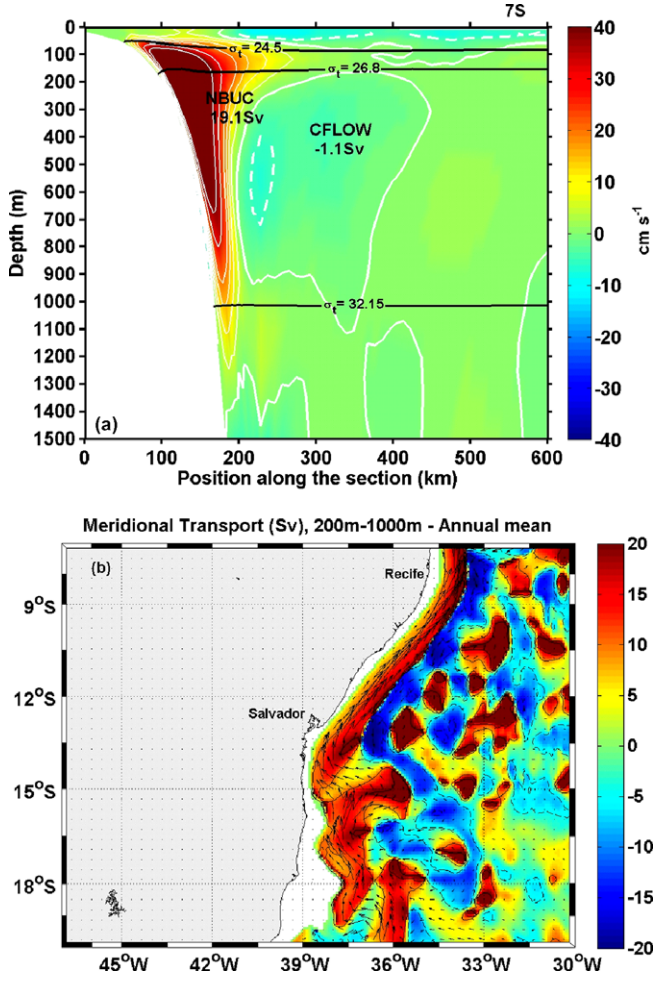

Fig. 9. Annual averaged (2005–2007) meridional current (cm s^{-1}) and transport (in Sv) obtained by ROMS for: (a) the along zonal section (0–1500 m) at 7°S. Positive (negative) values indicated by solid (dashed) lines correspond to northward (southward) currents, (b) the depth averaged range 200–1000 m, where CFLOW is stronger.

ments obtained at 19°S show a BC confined to the upper 200 m depth, with a mean southward velocity of approximately 15 cm s^{-1} (Müller et al., 1998). The mean cross-shore section at 19°S obtained here from the 2005–2007 simulations (Fig. 8c) confirms the presence of a southward BC tight flow (less than 100 km) limited to the top 200 m. At 19°S east of the NBUC flow (6.7 Sv), one can find the upper part of the DWBC transporting cold waters southward (1.8 Sv) above σ_t = 32.15 kg m^{-3} (Fig. 8c).

In our simulation, the sSEC bifurcation reaches its southernmost position in MJJ and its northernmost in OND, which corresponds, respectively, to the months of July (southernmost) and November (northernmost) found in the climatological runs of Rodrigues et al. (2007). Furthermore, a time variation of the model outputs indicates (Fig. 10) that the NBUC system strengthens around May 2006 and May 2007, *i.e.* when the sSEC bifurcation reaches its southernmost position, while the BC transport is decreasing at that time until March 2006, when it is practically null. On the other hand, maximum southward BC transports are verified during January 2006 as well as in January 2007 and March 2007, just after the period when sSEC bifurcation reaches its lowest latitudes, with a minimum northward NBUC flow in December 2005 and October/December 2006 (Fig. 10).

The depth dependence of the sSEC bifurcation latitude is abridged in Fig. 11a and b. In these figures, the sSEC bifurcation is represented by a white line, where the averaged (2005–2007) MJJ and OND meridional velocity (spatially averaged within a 1° longitude band off the Brazilian coast) is zero. The white areas in Fig. 11a and b represent the Vitória-Trindade Ridge and Abrolhos

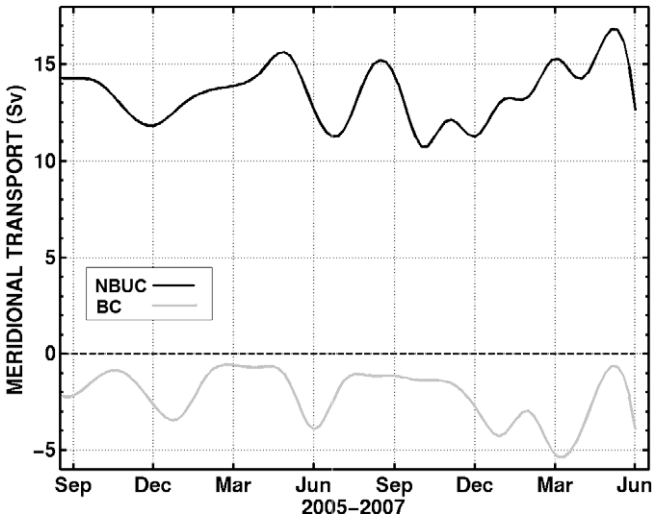

Fig. 10. Interannual variability of the North Brazil Undercurrent (NBUC) transport along 8°S (from the surface to 400 m), and Brazil Current (BC) transport along 19°S (from the surface to 400 m), obtained from ROMS simulations for the period of September 2005 to July 2007. Positive (negative) values indicated by the black (gray) line correspond to northward (southward) transports of NBUC (BC).

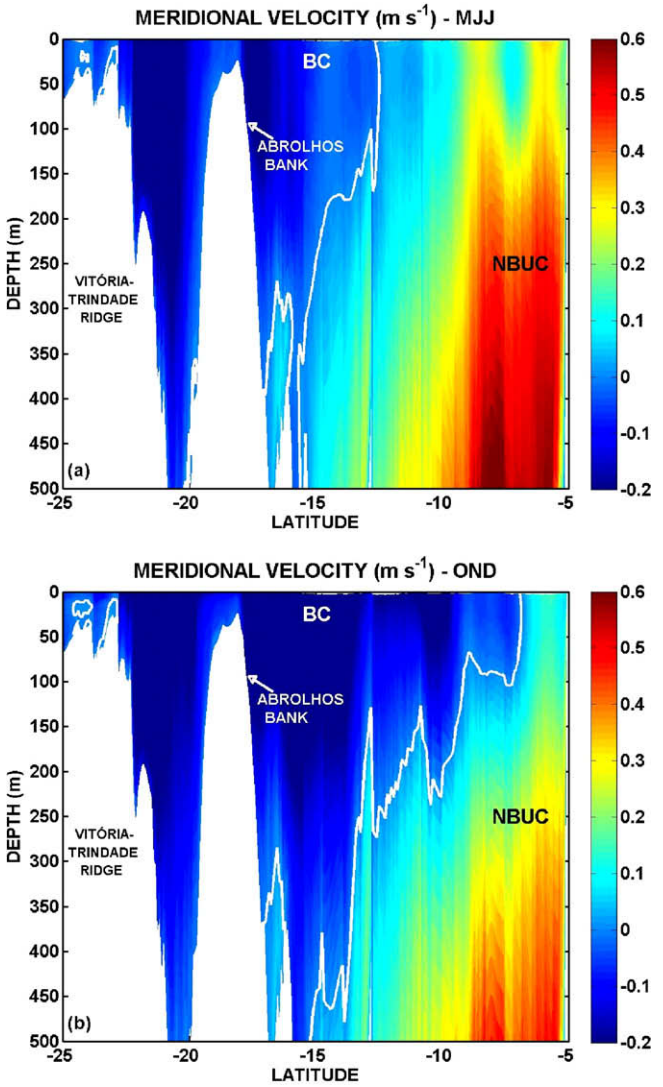

Fig. 11. Seasonal averaged (three months, 2005–2007) meridional velocity (m s^{-1}) obtained from the ROMS simulation for (a) MJJ and (b) OND. The velocities are averaged within a 1° longitude band off of the Brazilian coast. The white line is the contour of zero velocity that represents the bifurcation of the sSEC. The white areas represent the Vitoria-Trindade Ridge and Abrolhos Bank.

Bank. ROMS also agrees well with the numerical findings of Harper (2000), Malanotte-Rizzoli et al. (2000) and Rodrigues et al. (2007), indicating a poleward depth increase of the sSEC bifurcation along the Brazilian coastline. Averaged MJJ results in Fig. 11a show that the bifurcation varies from near the surface at 13°S to 500 m depth at the model boundary at 24°S. During this period, the NBUC is strengthened and the BC weakened. In contrast, the OND averaged results indicate that the bifurcation shifts southward from 8°S at the surface layers to 20°S at 500 m depth, when a weaker NBUC and stronger BC are observed (Fig. 11b)

This southward deepening of sSEC bifurcation along the shoreline results in a similar poleward depth increase of the NBUC cores, as verified in the 8°S, 14°S and 19°S transects (Fig. 8a–c). These numerical results have been also detected in field measurements. Stramma and England (1999) and Rodrigues et al. (2007) showed from hydrographic data that the SEC bifurcation takes place at 14–16°S in a near-surface layer (top 100 m), then at 14–20°S in the layer between 100 and 500 m, and at 21–26°S in the AAIW (500–1200 m). Wienders et al. (2000) also used hydrographic data to indicate that the SEC bifurcation latitude is 14°S at the surface, 24°S in the 400–500 m layer and around 26°S–28°S in the AAIW. More recently, the annual mean dynamic height and geostrophic flow charts generated by Rodrigues et al. (2007) from CTD and bottle data (Curry, 1996) confirmed the poleward shift of the sSEC with increasing depth.

5.3. Coupling westward sSEC and wind stress

The zonal current and transport averaged from September 2005 to July 2007 along the PIRATA-SWE array (Fig. 1) indicate how the southern part of the SEC extends before reaching the western continental boundary (Fig. 12a). Indeed, we note a complex succession of more powerful westward systems. From south to north, we find two near-surface cores of −8.5 and −2.9 Sv, corresponding to the broad and relatively weak sSEC westward flow between 10°S and 19.5°S (Stramma, 1991; Stramma and Schott, 1999; Lumpkin and Garzoli, 2005). More to the north, in the vicinity of the northern PIRATA mooring, a third westward core of −2.8 Sv surfaces as the southernmost part of the cSEC (Lumpkin and Garzoli, 2005). ROMS results also point out a less powerful near-surface eastward core of 1.25 Sv located between sSEC and cSEC. Other subsurface narrow eastward circulations may reach the whole water column between 200 and 1200 m depth (not fully shown in Fig. 12a).

According to this ROMS simulation, the mean westward transport between 8°S–30°W and 19°S–34°W, corresponding to the sum of the sSEC and cSEC, is −14.9 Sv for the upper 400 m, which agrees well with previous observations and numerical studies. For instance, the hydrographic data used by Stramma (1991) showed a westward SEC transport of about −20 Sv along 30°W for the upper 500 m comprised between 3°S and 19°S. Furthermore, the recent climatological simulations of Rodrigues et al. (2007) indicate an annual mean westward SEC transport between 6°S and 22°S of −15 Sv along the 30°W meridian and down to 400 m. These authors found maximum SEC transports during JFM of about −15.6 Sv, and minimum flows of −14.0 Sv during MJJ. September 2005 to July 2007 monthly-averaged westward transport (0–400 m depth) obtained from the ROMS simulation across the PIRATA-SWE moorings (Fig. 12b) shows large interannual and intraseasonal variability. The weakest westward transport (~10–11 Sv) is noted in mid-2006, while the strongest westward SEC transport

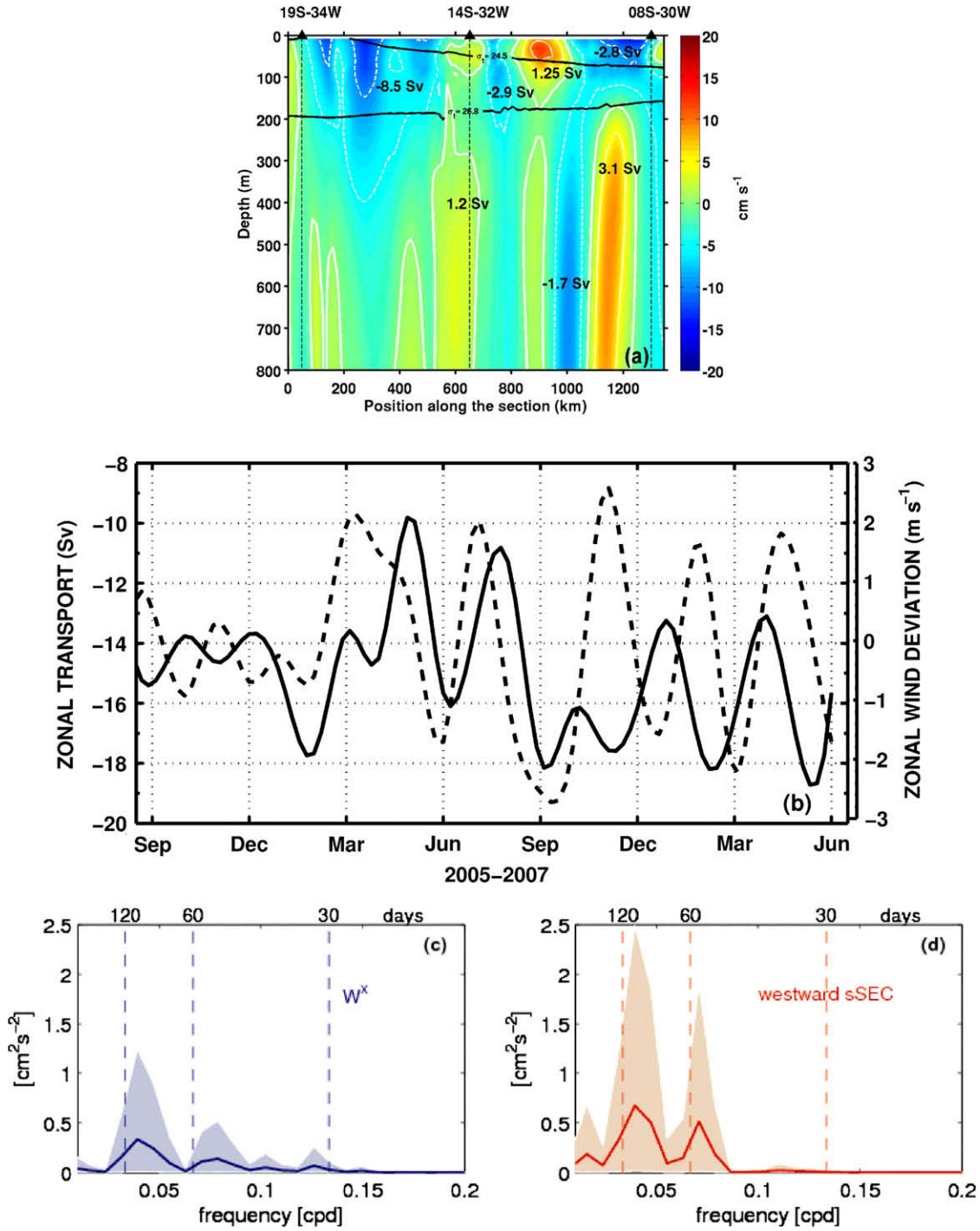

Fig. 12. (a) Mean annual volume transport averaged across the section along the PIRATA-SWE array between 8°S–30°W and 19°S–34°W. Positive (negative) values indicated by the solid (dashed) lines correspond to eastward (westward) currents. The two horizontal solid black lines indicate the 24.5 and 26.8 sigma-*t* values (in kg m^{-3}), respectively. (b) Time evolution (September 2005–June 2007) of the westward SEC transport (0–400 m depth) obtained from ROMS simulations along the PIRATA-SWE array (solid line), and the QuickSCAT zonal wind speed anomalies over the model domain (dashed line). The variance spectra for: (c) the zonal wind and (d) westward sSEC transport. The confidence levels are indicated by shaded areas in both spectra.

(~18–19 Sv) occurs in February 2006, and three times from September 2006 to June 2007. The time evolution (September 2005–June 2007) of the QuickSCAT zonal wind speed anomalies over the model domain is also plotted in Fig. 12b. One positive difference is weaker westward zonal winds than the mean, while negative deviation values indicate monthly zonal winds greater than the mean of zonal wind for the simulation period. Positive zonal wind anomalies are associated with a decrease in the upper transport of SEC, with time lags between zero and two months. These values occur in April 2006, July 2006, November 2006, February 2007 and April 2007 (Fig. 12b). Minimal SEC transports are observed in May 2006, August 2006, January 2007 and April 2007. On the other hand, the negative zonal wind anomalies in Fig. 12b (December and January 2006, August and September 2006, January 2007, March 2007), are followed by an increase in the SEC transport, which is observed in February 2006, September

2006, February 2007 and April 2007. In Fig. 12c and d the zonal wind speed anomalies over the model domain are correlated with westward sSEC transport (0–400 m depth) obtained from the ROMS simulation across the PIRATA-SWE (September 2005 to June 2007). Since the interest here is in the seasonal signals, a 30–180 day band-pass filter was applied to both the atmospheric and the modeling data to be compared. For the cross-correlation field, the variance-preserving spectra are constructed for the area with higher cross-correlation. The confidence levels are indicated by shaded areas in both spectra. The spectral analysis points out the signal periodicity of both datasets. The calculated maximum cross-correlation between zonal wind and westward transport is 0.51. The spectral analyses show two dominant signals at approximately 90 and 50 day periods for both zonal wind speed and sSEC transport (Fig. 12c and d, respectively). In addition to seasonal effects, these ocean signals may also represent the westward propagation of Rossby waves, as evidenced in the mooring measurements and analyses of Schott et al. (2005) and Schuckmann (2006).

6. Summary and conclusions

The primary motivation of this study was to evaluate and validate a high-resolution regional oceanic model in the southwestern tropical Atlantic. Until now, that region has been less studied, although it is of real interest for the global ocean inter-hemispheric heat transport. In the shallow waters, for instance, this is the region of the divergence of the SEC, which feeds many northward and southward currents along the western boundary. This is also a region of complex links between the climatic variability of SST, the heat content of the upper layers, atmospheric convective systems and precipitation on the adjacent continent, especially over northeastern Brazil.

Using the ROMS ocean model, we were particularly interested in evaluating the capacity of this model to reproduce instantaneous meso-scales oceanic dynamics. This first analysis focuses on intraseasonal and interannual conditions for the 2005–2007 period. After checking that ROMS makes it possible to correctly capture the meso-scale phenomena illustrated by instant SST patterns, numerical temperature values issued from a ROMS simulation were compared to vertical profiles obtained for the first two years of available data from the recently deployed PIRATA-SWE buoys. Comparisons between simulated temperature and *in-situ* temperature data agree well for the first 500 m ocean layer.

The first outputs of ROMS confirm the extreme complexity of the oceanic circulation in this area. This is obviously the case along the western continental boundary, where many alongshore currents coexist and can interact. Simulated Sea Surface elevation (SSH) and the derived surface Eddy Kinetic Energy (EKE) show good resemblance to AVISO Rio05 data, with the highest values (greater than 50 $cm^2\ s^{-2}$) found in cSEC and the NBUC/BC areas.

The interannual numerical results indicate a close relationship between SEC and the western boundary currents flowing along the Brazilian edge. When the sSEC bifurcation reaches its southernmost position (MJJ), the northward NBUC transport is stronger (May 2006, 2007) and the BC transport decreases. Otherwise, maximum southward BC flows are verified during January 2006 and January/March 2007, with minimum northward NBUC flows in December 2005 and October/December 2006, during the period when the sSEC bifurcation reaches its lowest latitudes (OND).

Along the section delineated by the PIRATA-SWE moorings, we highlighted the existence of three strong near-surface westward currents alternating with two weak eastward currents on a yearly average. Although the annual net mass transport across this PIRATA track is usually westward (14.9 Sv for the upper 400 m), this indicates that geostrophic computations using only the density profiles measured by the three PIRATA-SWE sites are somewhat misfit. This situation is worsened because the vertical measurements of salinity on the ATLAS moorings are presently limited to only four levels within the 0–120 m upper layer. This implies that for a continuous observation of the ocean dynamics in this area, it will be necessary to not only upgrade the vertical sampling of the PIRATA-SWE network, but also to implement other adapted systems.

The evaluation of this high-resolution regional ocean simulation shows the capability of the model in reproducing the known ocean dynamics in the region and their variability. We note that this has been achieved for a relatively long period and as a free run (*i.e.* without the need to artificially restore the model solution towards observations). Hence, we can now analyze this model solution in order to rigorously diagnose the dynamical balances and eddy dynamics.

In the future, this model could be improved by using a higher resolution to resolve smaller scales, by using improved turbulence closure schemes, or by using better surface forcing or lateral boundary conditions. Using the nesting capability of ROMS (Penven et al., 2006), we can now resolve explicitly the fast propagating signals across the whole tropical Atlantic while addressing the coastal response in the southwestern region. This model evaluation is a necessary step before coupling it to ecosystem (Koné et al., 2005), sediment (Blaas et al., 2007) and fishery (Lett et al., 2008) models, depending on the application needs.

For the regional climate of Northeast Brazil, this model could be fully dynamically coupled to a regional atmospheric model (Marchesiello et al., 2008). It could also be run in real-time to provide a decision-making tool for policy makers (Marchesiello et al., 2008).

Acknowledgements

This work is part of the CNPq-IRD Project "Climate of the Tropical Atlantic and Impacts on the Northeast" (CATIN), CNPq Process 492690/2004-9. M. Silva wishes to thank CAPES/BRAZIL (Coordination for the Improvement of Higher Education Staff) for scholarship support. C. Lentini also wishes to thank CNPQ (Grant 478398/2006-9) for its financial support.

Appendix A

Most criteria used to determine the MLD in the ocean require that the deviation of the temperature T (or density, σ_t) from its surface value be smaller then a certain fixed value (Sprintall and Tomczak, 1990; Brainerd and Gregg, 1995). The MLD is estimated as the depth at which density is equal to the sea surface value plus an increment $\Delta\sigma_t$ equivalent to a desired net decrease in temperature. For instance, Miller (1976) and Spall (1991) use $\Delta\sigma_t = 0.125\sigma_t(0)$ to determine the mixed layer depth, while Sprintall and Tomczak (1992) and Ohlmann et al. (1996) adopt $\Delta\sigma_t = 0.5\ ^\circ C(\partial\sigma_t/\partial T)$, where $\partial\sigma_t/\partial T$ is the coefficient of thermal expansion. Following Sprintall and Tomczak (1992), we evaluate the MLD in terms of temperature and density steps ($\Delta T = 0.5\ ^\circ C$ and $\Delta\sigma_t = 0.5\ ^\circ C(\partial\sigma_t/\partial T)$) from the SST and density ($T(0)$ and σ_t) obtained from the PIRATA and ROMS profiles:

$$\mathrm{MLD} = z\left(\sigma_t = \sigma_t(0) + \frac{\partial\sigma_t}{\partial T}\Delta T\right) \quad (1)$$

where $\partial\sigma_t/\partial T$ is calculated as a function of the surface temperature and salinity (Blanck, 1999).

References

Arhan, M., Mercier, H., Bourlès, B., Gouriou, Y., 1998. Hydrographic sections across the Atlantic at 7°30N and 4°30S. Deep Sea Research I 45, 829–872.

Blaas, M., Dong, C.M., Marchesiello, P., McWilliams, J.C., Stolzenbach, K.D., 2007. Sediment-transport modeling on Southern Californian shelves: a ROMS case study. Continental Shelf Research 27, 832–853.

Blanck, H.F., 1999. Using TOPEX Satellite El-Niño altimetry data to introduce thermal expansion and heat capacity concepts in chemistry courses. Journal of Chemical Education 76 (14), 1635–1646.

Bourlès, B., Molinari, R.L., Johns, E., Wilson, W.D., Leaman, K.D., 1999a. Upper layer currents in the western tropical North Atlantic (1989–1991). Journal of Geophysical Research 104 (C1), 1361–1375.

Bourlès, B., Gouriou, Y., Chuchla, R., 1999b. On the circulation in the upper layer of the western equatorial Atlantic. Journal of Geophysical Research 104, 21151–21170.

Bourlès, B., Lumpkin, R., McPhaden, M.J., Hernandez, F., Nobre, P., Campos, E., Yu, L., Planton, S., Busalacchi, A.J., Moura, A.D., Servain, J., Trotte, J., 2008. The PIRATA program: history, accomplishments, and future directions. Bulletin of the American Meteorological Society 89 (8), 1111–1125.

Brainerd, K.E., Gregg, M.C., 1995. Surface mixed and mixed layer depths. Deep Sea Research I 42, 1521–1543.

Campos, E.J.D., 2006. The equatorward translation of the Vitoria eddy in a numerical simulation. Geophysical Research Letters 33, L22607. doi:10.1029/2006GL026997.

Chaves, R.R., Nobre, P., 2004. Interactions between sea surface temperature over the South Atlantic Ocean and the South Atlantic Convergence Zone. Geophysical Research Letters 31, L03204. doi:10.1029/2003GL018647.

Curry, R.G., 1996. Hydrobase: A Database of Hydrographic Stations and Tools for Climatological Analysis. Woods Hole Oceanographic Institute. Technical Report 96-01, 50 pp.

da Silva, A.M., Young, C.C., Levitus, S., 1994. Atlas of surface marine data 1994, vol. 1, algorithms and procedures, NOAA Atlas NESDIS 6. U.S. Department of Commerce, NOAA, NESDIS, USA, 74 p.

De Almeida, R.A., Nobre, F.P., Haarsma, R.J., Campos, E.J.D., 2007. Negative ocean-atmosphere feedback in the South Atlantic Convergence Zone. Geophysical Research Letters 34, L18809. doi:10.1029/2007GL030401.

Evans, D.L., Signorini, S.R., Miranda, L.B., 1983. A note on the transport of the Brazil Current. Journal of Physical Oceanography 13, 1732–1738.

Ganachaud, A., 2003. Large-scale mass transport, water mass formation, and diffusivities estimated from World Ocean Circulation Experiment (WOCE) hydrographic data. Journal of Geophysical Research 108, L3213. doi:10.1029/2002JC001565.

Garzoli, S.L., Garrafo, Z., 1989. Transports, frontal motions and eddies at the Brazil–Malvinas currents confluence. Deep Sea Research 36, 681–703.

GODAE High Resolution Sea Surface Temperature Pilot Project—GHRSST-PP, 2007. http://www.ghrsst-pp.org/, online dataset, 04 June 2007.

Goes, M., Molinari, R., Silveira, I., Wainer, I., 2005. Retroflections of the North Brazil Current during February 2002. Deep Sea Research I 52, 647–667.

Gordon, A.L., Greengrove, C.L., 1986. Geostrophic circulation of the Brazil-Falklands confluence. Deep Sea Research I 33, 573–585.

Haidvogel, D.B., Arango, H.G., Hedström, K., Beckmann, A., Malanotte-Rizzoli, P., Shchepetkin, A.F., 2000. Model evaluation experiments in the North Atlantic basin: simulations in nonlinear terrain-following coordinates. Dynamics Atmosphere and Oceans 32, 239–281.

Harper, S., 2000. Thermocline ventilation and pathways of tropical-subtropical water mass exchange. Tellus 52A, 330–345.

Huang, B., Carton, J.A., Shukla, J., 1995. A numerical simulation of the variability in the tropical Atlantic Ocean, 1980–88. Journal of Physical Oceanography 25, 835–854.

Jochum, M., Malanotte-Rizzoli, P., Busalacchi, A., 2004. Tropical instability waves in the Atlantic ocean. Ocean Modelling 7, 145–163.

Koné, V., Machu, E., Penven, P., Andersen, V., Garçon, V., Fréon, P., Demarcq, H., 2005. Modeling the primary and secondary productions of the southern Benguela upwelling system: a comparative study through two biogeochemical models. Global Biogeochemical Cycles 19, GB4021. doi: 10.1029/2004GB002427.

Large, W.G., McWilliams, J.C., Doney, S.C., 1994. Oceanic vertical mixing: a review and a model with a nonlocal boundary layer parameterization. Reviews in Geophysics 32, 363–403.

Lett, C., Verley, P., Mullon, C., Parada, C., Brochier, T., Penven, P., Blanke, B., 2008. A Lagrangian tool for modelling ichthyoplankton dynamics. Environmental Modelling & Software 23, 1210–1214.

Liu, W.T., 2002. Progress in scatterometer applications. Journal of Oceanography 58, 121–136.

Lutjeharms, J.R.E., Penven, P., Roy, C., 2003. Modelling the shear edge eddies of the southern Agulhas Current. Continental Shelf Research 23, 1099–1115.

Lumpkin, R., Speer, K., 2003. Large-scale vertical and horizontal circulation in the North Atlantic ocean. Journal of Physical Oceanography 33, 1902–1920.

Lumpkin, R., Garzoli, S.L., 2005. Near-surface circulation in the tropical Atlantic Ocean. Deep Sea Research 52, 495–518.

McCready, P., Geyer, G.R., 2001. Estuarine salt flux through an isohaline surface. Journal of Geophysical Research 106, 11629–11637.

Malanotte-Rizzoli, P., Hedström, K., Arango, H.G., Haidvogel, D.B., 2000. Water mass pathways between the subtropical and tropical ocean in a climatological simulation of the North Atlantic. Dynamics of Atmosphere and Oceans 32, 331–371.

Marchesiello, P., McWilliams, J.C., Shchepetin, A., 2001. Open boundary conditions for long-term integration of regional oceanic models. Ocean Modelling 3, 1–20.

Marchesiello, P., Lefevre, J., Penven, P., Lemarie, F., Debreu, L., Douillet, P., Vega, A., Derex, P., Echevin, V., Dewitte, B., 2008. Keys to affordable regional marine forecast systems. La lettre trimestrielle Mercator Ocean 30, 38–48.

Miller, J.R., 1976. The salinity effect ion a mixed layer ocean model. Journal of Physical Oceanography 6, 29–35.

Miranda, L.B., Castro, B.M., 1981. Geostrophic flow conditions of the Brazil Current at 19°S. Ciência Interamericana 22, 44–48.

Moura, A., Shukla, J., 1981. On the dynamics of droughts in Northeast Brazil: observations, theory, and numerical experiments with a general circulation model. Journal of Atmospheric Science 38, 2653–2675.

Müller, T.J., Ikeda, Y., Zangenberg, N., Nonato, L.V., 1998. Direct measurements of the western boundary currents between 20°S–28°S. Journal of Geophysical Research 103, 529–543.

Nobre, P., Campos, E., Polito, P.S., Sato, O.T., Lorenzzetti, J.A., 2005. Brazilian Proposal for a PIRATA-SW Extension. Scientific Rationale, 44 pp.

OGCM-ECCO—Estimating the Circulation and Climate of the Ocean, 2007. http://ecco.jpl.nasa.gov/, online dataset, 12 September 2007.

Ohlmann, J.C., Siegel, D.A., Gautier, C., 1996. Ocean mixed layer depth heating and solar penetration: a global analysis. Journal of Climate 9, 2265–2280.

Olson, D.B., Podesta, G.P., Evans, R.H., Brown, O.B., 1988. Temporal variations in the separation of Brazil and Malvinas currents. Deep Sea Research I 35, 1971–1990.

Penven, P., Roy, C., Colin de Verdière, A., Largier, J., 2000. Simulation and quantification of a coastal jet retention process using a barotropic model. Oceanological Acta 23, 615–634.

Penven, P., Roy, C., Lutjeharms, J.R.E., Colin de Verdière, A., Johnson, A., Shillington, F., Fréon, P., Brundrit, G., 2001a. A regional hydrodynamic model of the Southern Benguala. South African Journal of Science 97, 472–476.

Penven, P., Lutjeharms, J.R.E., Marchesiello, P., Roy, C., Weeks, S.J., 2001b. Generation of cyclonic eddies by the Agulhas Current in the lee of the Agulhas Bank. Geophysical Research Letters 27, 1055–1058.

Penven, P., Debreu, L., Marchesiello, P., McWilliams, J.C., 2006. Application of the ROMS embedding procedure for the Central California Upwelling System. Ocean Modelling 12, 157–187.

Penven, P., Marchesiello, P., Debreu, L., Lefevre, J., 2008. Software tools for pre- and post-processing of oceanic regional simulations. Environmental Modelling and Software 23 (5), 660–662.

Peterson, R.G., Stramma, L., 1991. Upper-level circulation in the South Atlantic ocean. Progress in Oceanography 26, 1–73.

Polito, P.S., Cornillon, P., 1997. Long baroclinic Rossby waves detected by TOPEX/POSEIDON. Journal of Geophysical Research 102 (C2), 3215–3235.

Proehl, J., 1996. Linear instability of equatorial zonal flows. Journal of Physical Oceanography 26, 601–621.

Rao, V.B., de Lima, M.C., Franchito, S.H., 1993. Seasonal and inter-annual variations of rainfall over eastern Northeast Brazil. Journal of Climate 6, 1754–1763.

Rio, M.-H., Hernandez, F., 2004. A mean dynamic topography computed over the world ocean from altimetry, in situ measurements, and a geoid model. Journal of Geophysical Research 109, C12032. doi:10.1029/2003JC002226.

Rodrigues, R.R., Rothstein, L.M., Wimbush, M., 2007. Seasonal variability of the South Equatorial Current bifurcation in the Atlantic Ocean: a numerical study. Journal of Physical Oceanography 37, 16–37.

Schmid, C., Schafer, H., Podesta, G., Zenk, W., 1995. The Vitoria eddy and its relation to the Brazil Current. Journal of Physical Oceanography 25, 2532–2546.

Schott, F.A., Stramma, L., Fischer, J., 1995. The warm water inflow into the western tropical Atlantic boundary regime, spring 1994. Journal of Geophysical Research 100 (C12), 24745–24760.

Schott, F.A., Fischer, J., Stramma, L., 1998. Transports and pathways of the upper-layer circulation in the western tropical Atlantic. Journal of Physical Oceanography 28, 1904–1928.

Schott, F.A., Dengler, M., Zantropp, R., Stramma, L., Fischer, J., Brandt, P., 2005. The shallow and deep western boundary circulation of the South Atlantic at 5°–11°S. Journal of Physical Oceanography 35, 2031–2053.

Schuckmann, K., 2006. Intraseasonal variability in the southwestern and central tropical Atlantic ocean. Ph.D. Thesis Christian-Albrechts-Universität, Kiel, Germany, 148 p.

Servain, J., Busalacchi, A., Moura, A., McPhaden, A., Reverdin, G., Vianna, M., Zebiak, S., 1998. A pilot research moored array in the tropical Atlantic (PIRATA). Bulletin of the American Meteorological Society 79, 2019–2031.

Shchepetkin, A.F., McWilliams, J.C., 1998. Quasi-monotone advection schemes based on explicit locally adaptive dissipation. Monthly Weather Review 126, 1541–1580.

Shchepetkin, A.F., McWilliams, J.C., 2005. The regional oceanic modeling system (ROMS): a split-explicit, free-surface, topography-following-coordinate oceanic model. Ocean Modelling 9, 347–404.

She, J., Klinck, J.M., 2000. Flow near submarine canyons driven by constant wind. Journal of Geophysical Research 105, 28671–28694.

Silveira, I.C.A., Miranda, L.B., Brown, W.S., 1994. On the origins of the North Brazil Current. Journal of Geophysical Research 99, 22501–22512.

Smith, W.H.F., Sandwell, D.T., 1997. Global seafloor topography from satellite altimetry and ship depth soundings. Science 277, 1957–1962.

Spall, M.A., 1991. A diagnostic study of wind- and buoyancy-driven north Atlantic circulation. Journal of Geophysical Research 96, 18509–18518.

Sprintall, J., Tomczak, M., 1990. Salinity considerations in the oceanic surface mixed layer. Ocean Sciences Institute Rep. 36, University of Sidney, 170 pp.

Sprintall, J., Tomczak, M., 1992. Evidences of the barrier layer in the surface layer of the tropics. Journal of Geophysical Research 97, 7305–7316.

Stramma, L., Peterson, R.G., 1990. The South Atlantic Current. Journal of Physical Oceanography 20, 846–859.

Stramma, L., 1991. Geostrophic transport of the South Equatorial Current in the Atlantic. Journal of Marine Research 49, 281–284.

Stramma, L., Fischer, J., Reppin, J., 1995. The North Brazil Undercurrent. Deep Sea Research I 42, 773–795.
Stramma, L., England, M., 1999. On the water masses and mean circulation of the South Atlantic Ocean. Journal of Geophysical Research 104, 20863–20883.
Stramma, L., Schott, F., 1999. The mean flow field of the tropical Atlantic Ocean. Deep Sea Research B 46, 279–303.
Stramma, L., Rhein, M., Brandt, P., Dengler, M., Böning, C., Walter, M., 2005. Upper ocean circulation in the western tropical Atlantic in boreal fall 2000. Deep Sea Research 52, 221–240.
Talley, L.D., 2003. Shallow, intermediate, and deep overturning components of the global heat budget. Journal of Physical Oceanography 33, 530–560.
Wienders, N., Arhan, M., Mercier, H., 2000. Circulation at the western boundary of the south and equatorial Atlantic. Journal of Marine Research 58, 1007–1039.